ACS APPLIED MATERIALS & INTERFACES

Research Article

www.acsami.org

$NiCo_2S_4$@graphene as a Bifunctional Electrocatalyst for Oxygen Reduction and Evolution Reactions

Qiao Liu,[†,‡] Jutao Jin,[†,‡] and Junyan Zhang*[,†]

[†]Lanzhou Institute of Chemical Physics, Chinese Academy of Sciences, Lanzhou 730000, China

[‡]University of Chinese Academy of Sciences, Beijing 100049, China

Supporting Information

ABSTRACT: Here, the hybrid of $NiCo_2S_4$ nanoparticles grown on graphene in situ is first described as an effective bifunctional nonprecious electrocatalyst for oxygen reduction reaction (ORR) and oxygen evolution reaction (OER) in the alkaline medium. $NiCo_2S_4$@N/S-rGO was synthesized by a one-pot solvothermal strategy using $Co(OAc)_2$, $Ni(OAc)_2$, thiourea, and graphene oxide as precursors and ethylene glycol as the dispersing agent; simultaneously, traces of nitrogen and sulfur were double-doped into the reduced graphene oxide (rGO) in the forms of pyrrolic-N, pyridinic-N, and thiophenic-S, which are often desirable for metal-free ORR catalysts. In comparison with commercial Pt/C catalyst, $NiCo_2S_4$@N/S-rGO shows less reduction activity, much better durability, and superior methanol tolerance toward ORR in 0.1 M KOH; it reveals higher activity toward OER in both KOH electrolyte and phosphate buffer at pH 7.0. $NiCo_2S_4$@graphene demonstrated excellent overall bicatalytic performance, and importantly, it suggests a novel kind of promising nonprecious bifunctional catalyst in the related renewable energy devices.

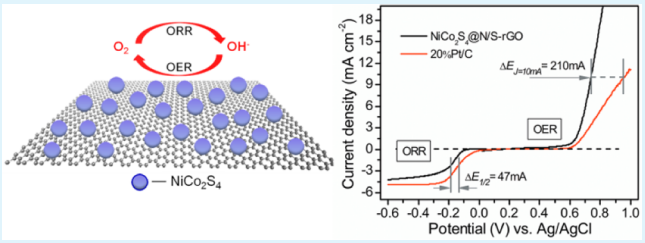

KEYWORDS: *cobalt sulfide, graphene, oxygen reduction, oxygen evolution, nonprecious electrocatalyst, doping effect, bifunctional catalyst, fuel cell*

1. INTRODUCTION

Oxygen reduction reaction (ORR) on the cathode is a decisive issue for fuel cells, while oxygen evolution reaction (OER) on the anode is the challenging energy storing reaction of water splitting and solar fuel synthesis. However, both reactions are complicated for multielectron transfer, leading to the sluggish kinetics. Catalysts are vital to "lubricate" these rigid processes. Thereby, the development of the bifunctional electrocatalyst for both ORR and OER (namely, bicatalyst) is at the heart of the key renewable-energy technology, such as metal-air batteries,[1] and unitized regenerative fuel cells (URFCs).[2] Currently, Pt functions as the best ORR catalyst,[3,4] but its OER activity is unsatisfactory.[5] Pt alloys, such as Pt/Ir[6−8] and Pt/Au,[1] were investigated as promising bicatalysts. However, the low abundance, prohibitive cost, and declining activity pose critical challenges for the practical use of the Pt-based catalysts. Therefore, it is imperative to search for the efficient and robust bicatalysts based on abundant nonprecious metals for the widespread applications.

Various nonprecious materials exhibit excellent catalytic activity for ORR[9] or OER,[10] while those as bicatalysts for both ORR and OER are rarely reported. First row transition metal chalcogenides, such as oxides,[11,12] sulfides,[13−16] and selenides,[17,18] have been extensively studied as ORR catalysts, but only transitional metal oxides,[19−22] namely, the Me-O system, were studied as bicatalysts. In particular, single or complex oxides of Mn,[3,9,21] Co,[19−22] and Ni[23] have been demonstrated as the effective bicatalysts in alkaline electrolytes. Lately, nonprecious transition-metal sulfides (Me-S) and selenides (Me-Se) have attracted intensive interest owing to their noble-metal-like catalytic properties.[24,25] For instance, nanostructured $CoSe_2$ was reported with excellent OER activity in the alkaline environment.[26] However, to the best of our knowledge, there is no report on Me-S- or Me-Se-based bicatalysts for both ORR and OER. Striving for the achievement of the low-cost and high-efficient bicatalysts, it is expected for one to explore a new material system based on all chalcogenides of transition metals. Co-S, including Co_3S_4,[13] CoS_2,[16] $Co_{1-x}S$,[15] etc., was regarded as one kind of the most active ORR catalysts among all chalcogenides, while Ni doped Co-S of thiospinel type (such as $NiCo_2S_4$) displayed higher ORR activity than the binary Co-S system.[27] To date, despite abundant research on Ni- and Co-S ORR catalyst, the investigations of their OER activity and even bicatalytic performance are still scarce. Herein, we report a Ni-Co-S bicatalyst and the reduced graphene oxide (rGO) was introduced as the synergist. Via a facile one-pot solvothermal method, the hybrid of $NiCo_2S_4$ nanoparticles in situ grown on N and S codoped rGO ($NiCo_2S_4$@N/S-rGO) was synthesized from metal salts, thiourea, and graphene oxide in the medium of ethylene glycol (EG). With regard to its great overall electrocatalytic performance toward both ORR and OER, the

Received: March 2, 2013
Accepted: May 11, 2013
Published: May 11, 2013

   dx.doi.org/10.1021/am4007897 | ACS Appl. Mater. Interfaces 2013, 5, 5002−5008

sulfide of Ni-Co is considered as a novel and promising nonprecious bifunctional oxygen catalyst for URFCs.

2. EXPERIMENTAL SECTION

2.1. Synthesis of $NiCo_2S_4$@N/S-rGO. The graphene oxide (GO) was prepared via an improved method,[28] and the detail was described in the Supporting Information. In a typical synthesis of $NiCo_2S_4$@N/S-rGO, $Co(OAc)_2$ (0.3 mmol) and $Ni(OAc)_2$ (0.15 mmol) were dissolved in 30 mL of GO/EG suspension and stirred at 80 °C for 2 h. Then, thiourea (0.9 mmol) was introduced into the above suspension, and after transferring the mixture to an autoclave (40 mL), the solvothermal reaction was followed at 200 °C for 6 h. The resulted product was collected by filtration, washed with plenty of deionized water, and lyophilized at last.

To study the priority of cobalt or nickle sulfides to the bicatalytic activity, Ni_3S_4@N/S-rGO and Co_3S_4@N/S-rGO were prepared through the same procedure as $NiCo_2S_4$@N/S-rGO, except for the molar ratio of metal precursors vs thiourea being 0.5. For comparisons, rGO, N/S-rGO, and free $NiCo_2S_4$ were prepared under the same conditions. The $NiCo_2S_4$ and N/S-rGO physical mixture was obtained by sonicating free $NiCo_2S_4$ and N/S-rGO mixture by the mass ratio of 5:2. $Ni_xCo_{3-x}S_4$@N/S-rGO was also prepared through the same steps as $NiCo_2S_4$@N/S-rGO just by varying the molar ratio of $Ni(OAc)_2$/$Co(OAc)_2$ as 2, 1, and 0.5.

2.2. Structural Characterization. The samples were pressed to thin films for powder X-ray diffraction (XRD) detections on a Rigaku B/Max-RB X-ray diffractometer with a nickel filtrated Cu Kα radiation (Cu Kα, λ = 1.5406). Transmission electron microscopy (TEM) images, high-resolution TEM (HRTEM) images, the corresponding selected area electron diffraction (SAED) patterns, and the energy dispersive spectroscopy (EDS) spectra were taken on a Tecnai-G2-F30(300 keV) field-emission TEM (FE-TEM). X-ray photoelectron spectroscopy (XPS) spectra were collected using a VG Scientific ESCALAB210-XPS photoelectron spectrometer with an Mg Kα X-ray resource.

2.3. Electrochemical Measurements. The electrochemical tests were carried out on a AutoLab workstation (μ Autolab III) assembled with a model of an ATA-1B rotational system, using a three-electrode electrochemical cell. The sample coated glass carbon (GC) electrode, a silver chloride electrode, and a platinum pole were used as working, reference, and counter electrode, repectively. The working electrode was prepared as follows: 100 μL of 5 wt % Nafion solution was added to 1 mL of 4:1 v/v water/ethanol, and then, 4 mg of the catalyst was dispersed in it by sonicating in an ice–water bath to obtain a homogeneous ink. Then, 5 μL of the catalyst ink was loaded onto a GC electrode of 3 mm in diameter (the catalysts loading was ~0.283 mg cm^{-2} for all samples). A commercial 20%Pt/C electrode was also preapred for comparison.

The ORR performance was first investigated by cyclic voltammetry (CV) in Ar and O_2-saturated 0.1 M KOH at room temperature, with a sweep rate of 20 mV s^{-1}. Linear sweep voltammetry (LSV) was conducted under constant O_2 gas flow, with a sweeping rate of 5 mV s^{-1} in the potential range of 0.1 to −0.6 V vs Ag/AgCl. The OER avtivities of all samples were investigated by the LSV method, with the sweep rate of 10 mV s^{-1} in 0.1 M KOH and 0.1 M phosphate buffer at pH 7.0 (PBS7.0). All data were collected after the constant and steady curves were obtained.

3. RESULTS AND DISCUSSION

$NiCo_2S_4$@N/S-rGO hybrid was prepared by a one-pot solvothermal approach using $Co(oAc)_2$, $Ni(oAc)_2$, thiourea, and GO as precursors in polyol (such as EG) medium. The polyol method is usually employed to synthesize nanosized materials.[29] It is known that a catalyst with amorphous or nanocrystalline phase would be rendered a great performance on account of abundant accessible active sites.[30,31] During the reaction, EG acts as a mild reductant to get rGO and also the solvent with a chelating effect, which avoids agglomeration of nanoparticles; GO provides large amounts of defects/functional groups as nucleation sites for in situ growth of $NiCo_2S_4$ nanocrystals. Thiourea is intended for the formation of metal sulfides but, interestingly, also induces double doping of N and S into rGO networks. The solvothermal procedure is of significant importance, affording the crystallization of $NiCo_2S_4$ nanoparticles (NPs), the reduction of GO, the doping of N/S in rGO, and the final formation of $NiCo_2S_4$@N/S-rGO hybrid.

TEM images (Figure 1a,b) of as-synthesized hybrid clearly reveal that metal sulfide NPs (~4−8 nm in size) are selectively

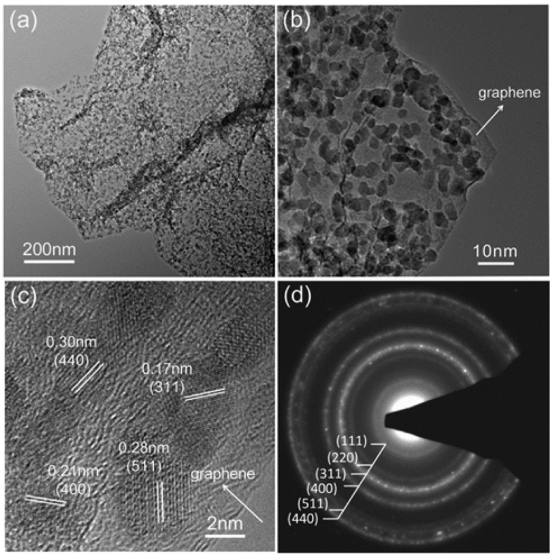

Figure 1. (a, b) The low-magnification and (c) high-magnification TEM images of $NiCo_2S_4$@N/S-rGO. (d) Corresponding SAED pattern of $NiCo_2S_4$ nanocrystals grown on graphene sheets.

and uniformly decorated on graphene sheets without detachment and aggregation. Lattice fringes in HRTEM image (Figure 1c) and the SEAD pattern (Figure 1d) are well consistent with each other, both showing (440), (511), (400), and (311) planes of $NiCo_2S_4$ (ICDD PDF card No.20-0782). The XRD pattern (Figure 2a), in a good agreement with the above results, further confirms the formation of $NiCo_2S_4$ nanocrystals. Element analyses from both EDS (Figure 2b) and XPS (Figure 2c) methods verify the atomic ratio of Co/Ni as about 2 in the hybrid. Therefore, the as-prepared material is the hybrid of $NiCo_2S_4$ NPs anchored on graphene.

In addition to the compositional information, XPS was also used to further investigate the electronic state of the present elements in the near surface region. First, it revealed ~4.52 at. % N, ~16.08 at. % S, ~4.95 at. % Co, and ~2.59 at. % Ni in $NiCo_2S_4$@N/S-rGO hybrid. The excessive S atoms for the formation of $NiCo_2S_4$ compound was accompanied with the presence of N atoms, which aroused a possibility of the simultaneous incorporation of N and S atoms into the hybrid material. It has been confirmed by the comparison of XPS spectra of $NiCo_2S_4$@N/S-rGO and N/S-rGO. For N/S-rGO, the survey spectrum showed the presence of C, N, S, and O (Figure 2d), without any other impurities; the atomic ratios of N, S, and O relative to C were ~0.072, 0.037, and 0.153, respectively. The N1s XPS spectrum of N/S-rGO seems nearly the same to that of $NiCo_2S_4$@N/S-rGO (Figure S1a, Supporting Information). Both N1s spectra can be further deconvoluted into three different signals, indicating the

dx.doi.org/10.1021/am4007897 | ACS Appl. Mater. Interfaces 2013, 5, 5002−5008

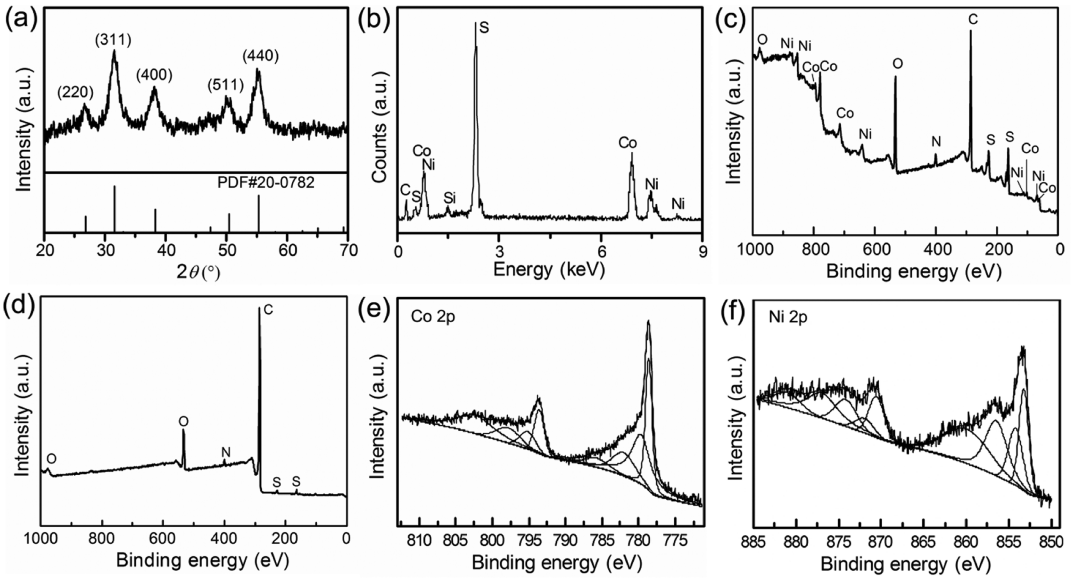

Figure 2. (a) XRD pattern and (b) EDS spectrum of $NiCo_2S_4$@N/S-rGO. (c, d) XPS survey spectra of $NiCo_2S_4$@N/S-rGO and N/S-rGO, respectively. (e, f) High resolution Co 2p and Ni 2p spectra of $NiCo_2S_4$@N/S-rGO hybrid, respectively.

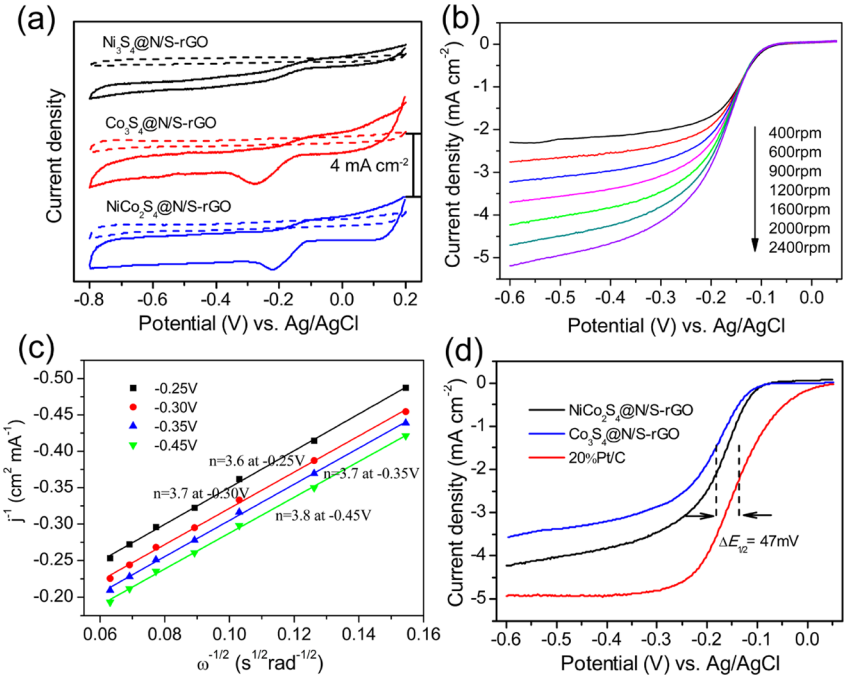

Figure 3. (a) CV curves of $NiCo_2S_4$@N/S-rGO, Co_3S_4@N/S-rGO, and Ni_3S_4@N/S-rGO in O_2-saturated (solid line) or Ar-saturated (dash line) 0.1 M KOH with a sweep rate of 20 mV s^{-1}. (b) RDE curves of $NiCo_2S_4$@N/S-rGO in O_2-saturated 0.1 M KOH with a sweep rate of 5 mV s^{-1} at different rotation rates. (c) Corresponding K-L plots at different potentials for RDE curves in (b). (d) RDE curves of 20%Pt/C, $NiCo_2S_4$@N/S-rGO, and Co_3S_4@N/S-rGO in O_2-saturated 0.1 M KOH at 1600 rpm with a sweep rate of 5 mV s^{-1}.

presence of pyridinic-N (398.5 eV), pyrrolic-N (400.0 eV), and ammonic-N (401.2 eV).[32,33] For the hybrid, the first two peaks (161.3 and 162.4 eV) on S 2p spectrum are doublet structures due to spin−orbit coupling (S $2p_{3/2}$ and S $2p_{1/2}$) in metal sulfide.[34] In addition, S $2p_{3/2}$ of thiophene at 164.3 eV was found for both the hybrid and pure N/S-rGO (Figure S1b, Supporting Information). Probed from S 2p spectrum of N/S-rGO, sulfur species exists in two distinct forms of thiophenic-S (aromatic C-S-C, 164.3 eV)[33] and thiolic-S (C-SH,163.2 eV).[35] The atomic ratio of $S_{thiophenic}/S_{thiolic}$ is about 1.35. The thiolic-S relates to the chemisorption of the breakdown product of thiourea, which is hard to be removed by continuous rinsing. Considering the evidence of pyrrolic- and pyridinic-N together with thiophenic-S, it is no doubt that traces of N and S are simultaneously incorporated into graphene networks.

The spectrum of Co 2p for the hybrid can be deconvoluted into two spin−orbit doublets and four shakeup satellites (Figure 2e). The first doublet at 778.4 and 793.3 eV and the second at 779.3 and 794.8 eV could be assigned to Co^{3+} and Co^{2+}, corresponding to a 2p level splitting of 15.1 and 15.5 eV, respectively.[36,37] The Co 2p spectrum of the hybrid looks similar to that of the individual $NiCo_2S_4$ with regard to their

dx.doi.org/10.1021/am4007897 | ACS Appl. Mater. Interfaces 2013, 5, 5002−5008

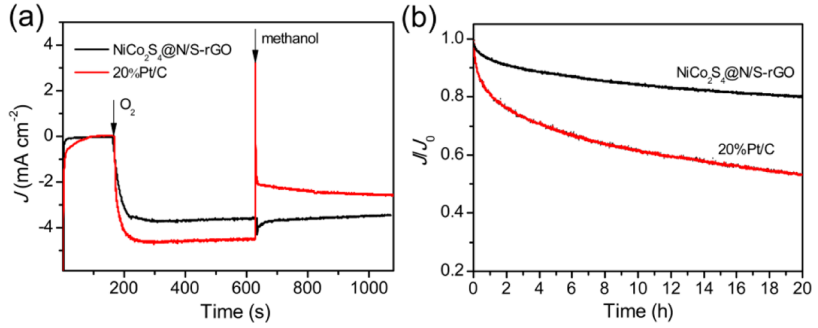

Figure 4. (a) Current−time chronoamperometric responses of $NiCo_2S_4$@N/S-rGO and 20%Pt/C at −0.45 V vs Ag/AgCl in 0.1 M KOH. The arrrows indicate the introduction of O_2 and methanol in sequence. (b) Current−time chronoamperometric responses of $NiCo_2S_4$@N/S-rGO and 20%Pt/C at a rotation rate of 1600 rpm for 20 h in O_2-saturated 0.1 M KOH.

close binding energy values and peak shapes (Figure S1c, Supporting Information). The spectral Co^{3+}/Co^{2+} ratio obtained from their respective main lines is ∼1.22 for the hybrid and ∼1.85 for free $NiCo_2S_4$. Figure 2f shows the Ni 2p spectrum of $NiCo_2S_4$@N/S-rGO. The main peak at 852.9 eV is comparable to the Ni^{2+} species found in Ni_3S_4.[38] The binding energy at 854.4 eV corresponds to the spin−orbit characteristic of Ni^{3+}.[39] The Ni^{2+}/Ni^{3+} ratio is ∼2.32 for the hybrid and ∼1.93 for free $NiCo_2S_4$ (Figure S1d, Supporting Information). Since there is a similarity of peak shape and a difference of peak intensity for both Co and Ni XPS spectra, it can be seen that the introduction of GO takes effect on the cationic distribution of $NiCo_2S_4$. However, abundant $NiCo_2S_4$ NPs grown on GO result in the depressed reduction of GO in turn, which is determined by the O/C values decreasing from 0.268 in the hybrid to 0.153 in N/S-rGO. This confirms the chemical coupling interaction between $NiCo_2S_4$ NPs and underlying N/S-rGO sheets.

It was reported that the transition metals with mixed valences could provide donor−acceptor chemisorption sites for the reversible adsorption of oxygen and realize high electric conductivity for electron hopping between cations with different valences.[19] Moreover, the interconnected GO sheets, as perfectly conducting channels,[40] could improve the electron transport rate from semiconducting catalyst NPs to the external circuit. These suggest that the structure of the mixed-valent Ni-Co-S compound coupled with rGO gives potentially high catalytic activity to $NiCo_2S_4$@N/S-rGO hybrid.

For better understanding of the electrocatalytic properties of $NiCo_2S_4$@N/S-rGO, Co_3S_4@N/S-rGO and Ni_3S_4@N/S-rGO were prepared as comparisons, and their respective structures were characterized by XRD and XPS methods (Figure S2, Supporting Information). Notably, Co^{3+}/Co^{2+} ratio is ∼1.29 in Co_3S_4@N/S-rGO, close to that in $NiCo_2S_4$@N/S-rGO, but for Ni_3S_4@N/S-rGO, Ni^{2+}/Ni^{3+} ratio is ∼0.257, far away from the value for $NiCo_2S_4$@N/S-rGO where Ni^{2+} is the dominant form of Ni species. The catalytic activities of the above three samples toward ORR were first examined by cyclic voltammograms (CV) in O_2- and Ar-saturated 0.1 M KOH at room temperature (Figure 3a). The ORR onset potential and peak potential of $NiCo_2S_4$@N/S-rGO are, respectively, at −0.11 and −0.22 V vs Ag/AgCl. These values are more positive than those of Co_3S_4@N/S-rGO (onset of −0.12 V and peak of −0.27 V) and Ni_3S_4@N/S-rGO (onset of −0.11 V and peak of −0.38 V). This indicates that Co_3S_4 gets preference for ORR catalyst over Ni_3S_4 and further suggests very poor activity of Ni^{3+} for ORR. The addition of Ni atoms has little effect on Co^{3+}/Co^{2+} distribution but has realized an improved ORR activity, which suggests that the doping of Ni^{2+}, rather than Ni^{3+}, would help in reducing the ORR overpotential of $NiCo_2S_4$.

The rotating-disk electrode (RDE) measurement was applied to reveal the ORR kinetics of $NiCo_2S_4$@N/S-rGO hybrid in O_2-saturated 0.1 M KOH (Figure 3b). The corresponding Koutecky−Levich (K-L) plots at various potentials show good linearity and near parallelism (Figure 3c), which suggests similar electron transfer numbers for ORR at different potentials. This also indicates first-order reaction kinetics with respect to the concentration of dissolved O_2.[41] The kinetic parameters can be analyzed on the basis of the K-L equations:

$$1/J = 1/J_K + 1/J_L = 1/J_K + 1/B\omega^{0.5} \quad (1)$$

$$B = nC \quad (2)$$

in which J, J_K, and J_L correspond to the measured current density and the kinetic- and diffusion-limiting current densities, respectively, ω is the angular velocity of the disk, n is the electron transfer number, and C is a constant relating to the concentration of O_2, kinematic viscosity of the electrolyte, etc. According to eqs 1 and 2, n and J_K can be obtained from the slope and intercept of the K-L plots, respectively. Taking 20% Pt/C as standard reference (Figure S3, Supporting Information), C can be calculated out as a system constant, where n is specified as 4.0 at each potential. In this way, n for $NiCo_2S_4$@N/S-rGO was achieved to be 3.6−3.8 throughout the tested potential range (Figure 3c). It suggests $NiCo_2S_4$@N/S-rGO favors a four electron ORR pathway. The calculated J_K value of 22.98 mA cm^{-2} at −0.45 V is lower than that of commercial 20%Pt/C (26.82 mA cm^{-2} at −0.45 V). It indeed exhibits inferior ORR activity to Pt-based catalyst, as shown in Figure 3d. In addition, $NiCo_2S_4$@N/S-rGO displays approximate half-wave potential ($E_{1/2}$) to Co_3S_4@N/S-rGO, and its $E_{1/2}$ value is 47 mV left apart from that of Pt/C (Ni_3S_4@N/S-rGO reveals negligible ORR activity, data not shown).

For the application in direct methanol fuel cells (DMFCs), the tolerance ability to the crossover effect is one of major concerns for ORR catalysts and also an obvious shortage of current Pt-based catalysts. The methanol crossover effect of $NiCo_2S_4$@N/S-rGO hybrid was evaluated at −0.45 V with a rotating rate of 1600 rpm. At this condition, the current density is the largest and not limited by mass transfer. The corresponding chronoamperometric responses of $NiCo_2S_4$@N/S-rGO and commercial 20%Pt/C are shown in Figure 4a. First, the introduction of O_2 significantly increased the ORR current for both catalysts, indicating great ORR activity of $NiCo_2S_4$@N/S-rGO and Pt/C. After adding methanol to the

dx.doi.org/10.1021/am4007897 | ACS Appl. Mater. Interfaces 2013, 5, 5002−5008

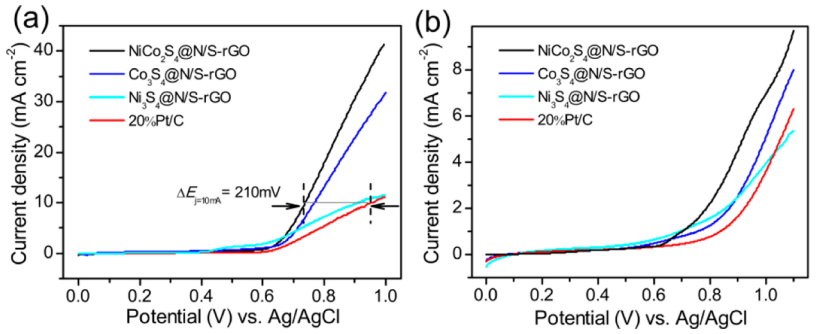

Figure 5. OER currents of $NiCo_2S_4$@N/S-rGO, Co_3S_4@N/S-rGO, Ni_3S_4@N/S-rGO, and commercial 20%Pt/C with a sweep rate of 10 mV s^{-1} in (a) 0.1 M KOH (pH~13) and (b) 0.1 M PBS7.0.

electrolyte (the resultant methanol concentration of 3M), $NiCo_2S_4$@N/S-rGO hybrid retained a stable current response, which suggests a good methanol tolerance. However, the corresponding current on Pt/C instantaneously decreased, indicating methanol oxidation reaction occurred, i.e., the degradation of commercial Pt/C catalyst.

The long-term stability of $NiCo_2S_4$@N/S-rGO and commercial Pt/C for ORR were also assessed by the chronoamperometric method under the same conditions as methanol tolerance measurement (Figure 4b). A high relative ORR current of 82% for $NiCo_2S_4$@N/S-rGO was retained after 20 h despite the initial drop of 10% in the first 2 h, whereas the ORR current response for Pt/C decreased nearly 50%. This confirms much better stability of $NiCo_2S_4$@N/S-rGO than that of Pt/C. It has been reported that nitrogen modified carbon-based catalysts exhibit great stability,[42,43] for its excellent mechanical and chemical stability relative to the carbon black in Pt/C, which could resist corrosion and thus effectively prevent the loss of active sites. For commercial Pt/C catalyst, except for the dissolution and sintering of Pt in working conditions, the poor stability of the carbon black also affects the loss of surface area of Pt nanoparticles following both particle sintering and release from the carbon support. We can infer that the high durability of $NiCo_2S_4$@N/S-rGO could be attributable to the stable structure of the heteroatom-doped graphene. Above all, in comparison with commercial Pt/C catalyst, $NiCo_2S_4$@N/S-rGO is insensitive to methanol and also has considerable durability, both of which are highly desirable for ORR catalysts in DMFCs.

As discussed above, $NiCo_2S_4$@N/S-rGO hybrid, prepared from the molar ratio of $Ni(OAc)_2/Co(OAc)_2$ at 0.5, enables a firm correlation between the Ni doping in Co_3S_4 and the electrocatalytic performance. It is required to investigate the influence of Ni doping degree on the ORR activity. The molar ratios of Ni/Co precursors were chosen at 2, 1, and 0.5, and the corresponding products were denoted as samples a, b, and c, respectively. XRD results (Figure S4a, Supporting Information) show sample a mainly consists of $CoNi_2S_4$ (PDF card No.24-0334) and Ni_3S_2 (PDF card No. 44-1418) and sample b is a mixture phase of Co_3S_4, $CoNi_2S_4$, or $NiCo_2S_4$ since it is too hard to be distinguished from the broad and asymmetric peaks. Only sample c is of a single phase of $NiCo_2S_4$, as shown in Figure 2a. Their LSV curves in the range of 0.05−0.6 V were compared in Figure S4b, Supporting Information. It can be seen that the increased ORR current density is accompanied with the decreased nickel proportion. However, sample b possesses comparable ORR activity to that of sample c. This indicates that the partial substitution by Ni atoms in the crystal lattice of Co_3S_4 (Ni/Co ratio ≤1) is very effective for the improvement of ORR kinetics. It also implies that $NiCo_2S_4$ exhibits higher intrinsic ORR activity than Co_3S_4 and $CoNi_2S_4$, suggesting the Ni doping extent is a crucial factor for optimizing the catalyst's ORR performance.

Now, the as-prepared $NiCo_2S_4$@N/S-rGO demonstrated great ORR performance; how about its OER activity? Then, the OER performance of $NiCo_2S_4$@N/S-rGO hybrid was estimated by polarization experiments in 0.1 M KOH and 0.1 M PBS7.0. In 0.1 M KOH, $NiCo_2S_4$@N/S-rGO displays notably greater OER current, as compared with all other samples (Figure 5a). When the applied potential is below 0.8 V vs Ag/AgCl, the current response inevitably corresponds to the oxidizing power of Co/Ni ions where the OER chemical is minimal; therefore, the actual OER current should be moderately reduced. However, to be sure, $NiCo_2S_4$@N/S-rGO reveals close OER activity to Co_3S_4@N/S-rGO but much better than Ni_3S_4@N/S-rGO and Pt/C. In PBS7.0, a similar trend was observed (Figure 5b), further confirming the potentially easier OER kinetics of $NiCo_2S_4$@N/S-rGO in both electrolytes. In brief, both ORR and OER activity increase in the order of Ni_3S_4@graphene, Co_3S_4@graphene, and $NiCo_2S_4$@graphene, suggesting the better bicatalytic activity of Co-S than Ni-S, and the improvement of bicatalytic activity resulted from the Ni doping effect.

The potential required for the current density of 10 mA cm^{-2} ($E_{j=10\ mA}$) is a matric relevant to solar fuel synthesis, commonly used to evaluate the OER activity.[5,20] As for $NiCo_2S_4$@N/S-rGO, $E_{j=10\ mA}$ is about 210 mV less positive than that of Pt/C in 0.1 M KOH. Our catalyst affords a current density of 10 mA cm^{-2} at a small overpotential of ~0.47 V, close to the best performance of the well-investigated Co_3O_4/graphene hybrid[20] and $CoSe_2/Mn_3O_4$ catalyst[26] reported at similar loadings. It is convenient to estimate the overall electrocatalytic activity and the reversibility of $NiCo_2S_4$@N/S-rGO as an oxygen electrode in alkaline electrolyte, by the variance matrices $\Delta(E_{j=10\ mA} - E_{1/2})$ between ORR and OER. The value was about 0.94 V for $NiCo_2S_4$@N/S-rGO whereas it was 1.10 V for 20%Pt/C. It has been demonstrated that $NiCo_2S_4$@N/S-rGO is potentially favorable to be a bifunctional oxygen catalyst.

In addition to the Ni doping effect discussed above, we also investigated how the coupling interaction between $NiCo_2S_4$ NPs and N/S-rGO affects the catalytic performance of the hybrid. A physical mixture was prepared with an approximate catalyst composition (~7:3 weight ratio of $NiCo_2S_4$ vs rGO) as comparison. N/S-rGO revealed pronounced ORR activity, but both onset potential (−0.21 V) and peak potential (−0.37 V) were more negative than that of the hybrid and the mixture

(Figure S5a, Supporting Information). It is likely related to the low doping amounts of nitrogen and sulfur atoms. Without heteroatom doping, the pure rGO has negligible activity for ORR (data not shown). The choice of thiourea results in simultaneous codoping of N and S in rGO, which is a hot subject recently for the pursuit of metal free ORR catalyst.[33] Besides, N/S-rGO may be a smart choice for constructing nanoelectronic devices for its possibility to modulate the electronic properties of GO sheets by adjusting the amounts and formats of sulfur and nitrogen introduced.

The physical mixture of $NiCo_2S_4$ NPs and N/S-rGO displayed an improved catalytic activity compared with each component alone but still inferior to the hybrid. This suggests that the high ORR catalytic activity of $NiCo_2S_4$@N/S-rGO is facilitated by the strong synergistic effect between $NiCo_2S_4$ NPs and N/S-rGO in the hybrid. Furthermore, the individual $NiCo_2S_4$ revealed smaller OER current response than the hybrid, while the mixture of $NiCo_2S_4$ and N/S-rGO showed much lower activity than the above two (Figure S5b, Supporting Information). It is thus inferred that the excellent OER activity of $NiCo_2S_4$@N/S-rGO hybrid is originated from $NiCo_2S_4$, where N/S-rGO serves as a synergist. Furthermore, the nanostructure of $NiCo_2S_4$ is considered to be critical to facilitate the OER process. Without graphene, as-prepared free $NiCo_2S_4$ is porous and cross-linked by loosely packed nanosheets (Figure S6, Supporting Information), which could provide abundant active sites and convenient mass-transfer channels. That can explain why free $NiCo_2S_4$ sample also shows obvious ORR activity despite its poor electric conductivity. Overall, for OER analyses, Ni doping effect and the synergistic effect between Me-S particles and graphene are not as significant as that found in the ORR process, which can be ascribed to the different active species for ORR and OER[5] in the same material. Also, the influence of the Ni doping degree on OER current response (Figure S4c, Supporting Information) indicates the Ni doping in Co_3S_4 would take positive effect on the improvement of both ORR and OER performance.

Much effort has been focused on the direction of improving turn over frequency (TOF) and the density of active site, which are the basic but primary factors determining the catalyst's performance.[9] This work as one of them tried to interpret a novel Me-S-based bicatalyst with excellent performance for both ORR and OER, in view of the following three points. The first and dominant factor is the doping effect. The preparation procedure has turned out to be effective for getting Ni doped Co_3S_4 and N/S codoped rGO. Both doping phenomena would contribute to the ORR activity, especially the Ni doping. The inclusion of Ni^{2+} in Co_3S_4 takes positive effect on the overall bicatalytic activity. Mixed-valence in Ni-Co-S nanocrystals is helpful for easier electron transfer and O_2 reversible absorption,[19] which bestow the enhanced TOF of single active site for both reactions in the alkaline medium. Another factor taken into account is the nanostructured nature of $NiCo_2S_4$ particles grown on rGO sheets. The nanosize and well-dispersion of $NiCo_2S_4$ depend on the chelating effect of EG and the chemical functionalities of GO. Interconnected GO sheets, except for anchoring and dispersing NPs, also serve as 3D diffusion channels to promote the mass transfer and highly conducting channels to improve the electron transfer on the electrode surface. The strong electron coupling interaction between $NiCo_2S_4$ NPs and rGO is the last but not the least factor for the enhanced ORR and OER performance, presumably due to the increasing utilization of active sites by the introduction of rGO. Further studies are necessary to understand the origins of the bifunctional activity of Me-S@graphene.

To the best of our knowledge, there were no reports about nonprecious Me-S as a bifunctional catalyst and even a direct OER catalyst.[44] Some typical weak acid anions, such as phosphate and borate ions, act as the proton acceptor and demonstrate high activity for OER process.[45−47] Just like them, sulfide ion is naturally associated with the observed excellent OER activity of $NiCo_2S_4$@N/S-rGO. It is believed that the propensity of metal ion dissolution usually correlates with ligand substitution, resulting in the formation of catalyst with an anion continuously.[46] It is plausible that the resolve/redeposition are driven by the oxidation of Co^{2+} and the interaction between sulfide ions and the fresh Co^{3+}. Thus, cobalt sulfide, or nickle sulfide, is capable of being an OER catalyst, and this assumption needs to be investigated thoroughly by much more experimental and theoretical analysis in the near future.

4. CONCLUSIONS

We have prepared $NiCo_2S_4$@N/S-rGO as a novel bicatalyst via a one-pot polyol method, using thiourea, metal acetates, and GO as precursors. Compared with Pt/C catalyst, $NiCo_2S_4$@N/S-rGO exhibits excellent overall electrocatalytic activity toward ORR and OER in alkaline electrolyte, and the long-term stability and methanol tolerance ability for ORR are outperformed as well. This is the first time that Me-S compound has been investigated as an effective bicatalyst, which provides a new choice for the design and fabrication of nonprecious bifunctional oxygen catalysts. Moreover, the high performance of the as-prepared hybrid is closely related to three factors, including doping effect and nanostructured $NiCo_2S_4$ as well as the strong synergetic coupling interaction at the interfaces of $NiCo_2S_4$ and graphene sheets. All these points are considered as promising strategies for improving the electrochemical performance of the current ORR and OER catalysts and even other advanced materials.

■ ASSOCIATED CONTENT

Supporting Information

Additional characterization data including XPS spectra of $NiCo_2S_4$@N/S-rGO, $NiCo_2S_4$, and N/S-rGO (Figure S1), XRD patterns and XPS analyses of Co_3S_4@N/S-rGO and Ni_3S_4@N/S-rGO (Figure S2), RDE curves and corresponding K-L plots of commercial 20%Pt/C (Figure S3), XRD patterns and LSV curves of samples at varying Ni/Co molar ratios (Figure S4), and the LSV curves of $NiCo_2S_4$@N/S-rGO, N/S-rGO, and $NiCo_2S_4$ and the physical mixture of $NiCo_2S_4$ and N/S-rGO (Figure S5). This material is available free of charge via the Internet at http://pubs.acs.org.

■ AUTHOR INFORMATION

Corresponding Author

*Phone: +86-931-4968295. Fax: +86-931-4968295. E-mail: zhangjunyan@licp.cas.cn.

Notes

The authors declare no competing financial interest.

■ ACKNOWLEDGMENTS

The authors greatly appreciate the financial support from the National Natural Science Foundation of China (50823008).

■ REFERENCES

(1) Lu, Y.-C.; Xu, Z.; Gasteiger, H. A.; Chen, S.; Hamad-Schifferli, K.; Shao-Horn, Y. *J. Am. Chem. Soc.* **2010**, *132*, 12170−12171.
(2) Chen, G.; Delafuente, D. A.; Sarangapani, S.; Mallouk, T. E. *Catal. Today* **2001**, *67*, 341−355.
(3) Arroyo-Ramírez, L.; Rodríguez, D.; Otaño, W.; Cabrera, C. R. *ACS Appl. Mater. Interfaces* **2012**, *4*, 2018−2024.
(4) Choi, S.-I.; Lee, S.-U.; Kim, W. Y.; Choi, R.; Hong, K.; Nam, K. M.; Han, S. W.; Park, J. T. *ACS Appl. Mater. Interfaces* **2012**, *4*, 6228−6234.
(5) Gorlin, Y.; Jaramillo, T. F. *J. Am. Chem. Soc.* **2010**, *132*, 13612−13614.
(6) Jung, H. Y.; Park, S.; Popov, B. N. *J. Power Sources* **2009**, *191*, 357−361.
(7) Kong, F.-D.; Zhang, S.; Yin, G.-P.; Wang, Z.-B.; Du, C.-Y.; Chen, G.-Y.; Zhang, N. *Int. J. Hydrogen Energy* **2012**, *37*, 59−67.
(8) Kong, F. D.; Zhang, S.; Yin, G. P.; Zhang, N.; Wang, Z. B.; Du, C. Y. *J. Power Sources* **2012**, *210*, 321−326.
(9) Chen, Z.; Higgins, D.; Yu, A.; Zhang, L.; Zhang, J. *Energy Environ. Sci.* **2011**, *4*, 3167−3192.
(10) Yamazaki, H.; Shouji, A.; Kajita, M.; Yagi, M. *Coord. Chem. Rev.* **2010**, *254*, 2483−2491.
(11) Cheng, F.; Su, Y.; Liang, J.; Tao, Z.; Chen, J. *Chem. Mater.* **2010**, *22*, 898−905.
(12) Matsumoto, Y.; Sato, E. *Mater. Chem. Phys.* **1986**, *14*, 397−426.
(13) Feng, Y.; He, T.; Alonso-Vante, N. *Chem. Mater.* **2008**, *20*, 26−28.
(14) Sidik, R. A.; Anderson, A. B. *J. Phys. Chem. B* **2006**, *110*, 936−941.
(15) Wang, H.; Liang, Y.; Li, Y.; Dai, H. *Angew. Chem., Int. Ed.* **2011**, *50*, 1−5.
(16) Zhu, L.; Susac, D.; Teo, M.; Wong, K.; Wong, P.; Parsons, R.; Bizzotto, D.; Mitchell, K.; Campbell, S. *J. Catal.* **2008**, *258*, 235−242.
(17) Gao, M. R.; Gao, Q.; Jiang, J.; Cui, C. H.; Yao, W. T.; Yu, S. H. *Angew. Chem., Int. Ed.* **2011**, *123*, 5007−5010.
(18) Zhao, D. J.; Zhang, S.; Yin, G. P.; Du, C. Y.; Wang, Z. B.; Wei, J. *J. Power Sources* **2012**, *206*, 103−107.
(19) Hamdani, M.; Singh, R.; Chartier, P. *Int. J. Electrochem. Sci.* **2010**, *5*, 556−577.
(20) Liang, Y.; Li, Y.; Wang, H.; Zhou, J.; Wang, J.; Regier, T.; Dai, H. *Nat. Mater.* **2011**, *10*, 780−786.
(21) Liang, Y.; Wang, H.; Zhou, J.; Li, Y.; Wang, J.; Regier, T.; Dai, H. *J. Am. Chem. Soc.* **2012**, *134*, 3517−3523.
(22) Nikolova, V.; Iliev, P.; Petrov, K.; Vitanov, T.; Zhecheva, E.; Stoyanova, R.; Valov, I.; Stoychev, D. *J. Power Sources* **2008**, *185*, 727−733.
(23) Rashkova, V.; Kitova, S.; Konstantinov, I.; Vitanov, T. *Electrochim. Acta* **2002**, *47*, 1555−1560.
(24) Gong, F.; Wang, H.; Xu, X.; Zhou, G.; Wang, Z.-S. *J. Am. Chem. Soc.* **2012**, *134*, 10953−10958.
(25) Wang, M.; Anghel, A. M.; Marsan, B.; Cevey Ha, N.-L.; Pootrakulchote, N.; Zakeeruddin, S. M.; Grätzel, M. *J. Am. Chem. Soc.* **2009**, *131*, 15976−15977.
(26) Gao, M.-R.; Xu, Y.-F.; Jiang, J.; Zheng, Y.-R.; Yu, S.-H. *J. Am. Chem. Soc.* **2012**, *134*, 2930−2933.
(27) Baresel, V. D.; Sarholz, W.; Scharner, P.; Schmitz, J. *Ber Bunsen-Ges.* **1974**, *78*, 608−611.
(28) Marcano, D. C.; Kosynkin, D. V.; Berlin, J. M.; Sinitskii, A.; Sun, Z.; Slesarev, A.; Alemany, L. B.; Lu, W.; Tour, J. M. *ACS Nano* **2010**, *4*, 4806−4814.
(29) Feldmann, C.; Jungk, H. O. *Angew. Chem., Int. Ed.* **2001**, *40*, 359−362.
(30) Arico, A. S.; Bruce, P.; Scrosati, B.; Tarascon, J.-M.; van Schalkwijk, W. *Nat. Mater.* **2005**, *4*, 366−377.
(31) Hocking, R. K.; Brimblecombe, R.; Chang, L.-Y.; Singh, A.; Cheah, M. H.; Glover, C.; Casey, W. H.; Spiccia, L. *Nat. Chem.* **2011**, *3*, 461−466.
(32) Morozan, A.; Jegou, P.; Jousselme, B.; Palacin, S. *Phys. Chem. Chem. Phys.* **2011**, *13*, 21600−21607.
(33) Wohlgemuth, S.-A.; White, R. J.; Willinger, M.-G.; Titirici, M.-M.; Antonietti, M. *Green Chem.* **2012**, *14*, 1515−1523.
(34) Wang, Z.; Pan, L.; Hu, H.; Zhao, S. *CrystEngComm* **2010**, *12*, 1899−1904.
(35) Wagner, C. D.; Riggs, W. W.; Davis, L. E.; Moulder, J. F.; Muilenberg, G. E. *Handbook of X-Ray Photoelectron Spectroscopy*; Perkin-Elmer Corporation: Eden Prairie, MN, USA, 1979.
(36) Bao, S. J.; Li, Y.; Li, C. M.; Bao, Q.; Lu, Q.; Guo, J. *Cryst. Growth Des.* **2008**, *8*, 3745−3749.
(37) Marco, J. F.; Gancedo, J. R.; Gracia, M.; Gautier, J. L.; Rios, E. I.; Palmer, H. M.; Greaves, C.; Berry, F. J. *J. Mater. Chem.* **2001**, *11*, 3087−3093.
(38) Yang, S.-L.; Yao, H.-B.; Gao, M.-R.; Yu, S.-H. *CrystEngComm* **2009**, *11*, 1383−1390.
(39) Zhang, H. T.; Wu, G.; Chen, X. H. *Mater. Lett.* **2005**, *59*, 3728−3731.
(40) Wakabayashi, K.; Takane, Y.; Sigrist, M. *Phys. Rev. Lett.* **2007**, *99*, 036601.
(41) Mayrhofer, K. J. J.; Strmcnik, D.; Blizanac, B. B.; Stamenkovic, V.; Arenz, M.; Markovic, N. M. *Electrochim. Acta* **2008**, *53*, 3181−3188.
(42) Liu, R.; Wu, D.; Feng, X.; Müllen, K. *Angew. Chem., Int. Ed.* **2010**, *49*, 2565−2569.
(43) Ma, G.; Jia, R.; Zhao, J.; Wang, Z.; Song, C.; Jia, S.; Zhu, Z. *J. Phys. Chem. C* **2011**, *115*, 25148−25154.
(44) Dimitrijevic, N. M.; Li, S.; Graetzel, M. *J. Am. Chem. Soc.* **1984**, *106*, 6565−6569.
(45) Esswein, A. J.; Surendranath, Y.; Reece, S. Y.; Nocera, D. G. *Energy Environ. Sci.* **2011**, *4*, 499−504.
(46) Kanan, M. W.; Nocera, D. G. *Science* **2008**, *321*, 1072−1075.
(47) Kanan, M. W.; Surendranath, Y.; Nocera, D. G. *Chem. Soc. Rev.* **2008**, *38*, 109−114.